

# VAR-3D: View-aware Auto-Regressive Model for Text-to-3D Generation via a 3D Tokenizer

Zongcheng Han

School of Computer Science and Technology  
Soochow University, Suzhou, China

Haoran Sun

School of Computer Science and Technology  
Soochow University, Suzhou, China

Dongyan Cao

School of Computer Science and Technology  
Harbin Institute of Technology, Harbin, China

Yu Hong\*

School of Computer Science and Technology  
Soochow University, Suzhou, China

## Abstract

Recent advances in auto-regressive transformers have achieved remarkable success in generative modeling. However, text-to-3D generation remains challenging, primarily due to bottlenecks in learning discrete 3D representations. Specifically, existing approaches often suffer from information loss during encoding, causing representational distortion before the quantization process. This effect is further amplified by vector quantization, ultimately degrading the geometric coherence of text-conditioned 3D shapes. Moreover, the conventional two-stage training paradigm induces an objective mismatch between reconstruction and text-conditioned auto-regressive generation. To address these issues, we propose View-aware Auto-Regressive 3D (VAR-3D), which integrates a view-aware 3D Vector Quantized-Variational AutoEncoder (VQ-VAE) to convert the complex geometric structure of 3D models into discrete tokens. Additionally, we introduce a rendering-supervised training strategy that couples discrete token prediction with visual reconstruction, encouraging the generative process to better preserve visual fidelity and structural consistency relative to the input text. Experiments demonstrate that VAR-3D significantly outperforms existing methods in both generation quality and text-3D alignment.

## Keywords

Text-to-3D, 3D Representation, Auto-regressive Modeling, Vector Quantization, Visual Supervision

## 1 Introduction

High-quality 3D generation is a fundamental challenge in computer vision, graphics, gaming, and immersive augmented and virtual reality systems. While auto-regressive transformers have achieved remarkable success in Large Language Models (LLMs) [1, 7, 17, 37, 57] and 2D generation [50, 54, 69], and Multimodal Large Language Models (MLLMs) [2, 20, 52], extending these advances to text-to-3D synthesis remains non-trivial. This difficulty stems from the complex structural nature of 3D data and the stringent requirement for global spatial consistency when translating sparse textual descriptions into dense geometric representations.

Recent research has explored diverse paradigms for 3D generation. Reconstruction-based approaches [25, 56] often struggle to infer plausible geometry from a single image, while methods leveraging 2D diffusion priors [10, 34, 47, 60] are frequently limited by

view inconsistency across synthesized images. Then, native 3D generative models [13, 14, 27, 29, 48, 53, 73] have shown strong potential, supporting both image and text. Nevertheless, these approaches still face challenges in representation efficiency, scalability, and semantic fidelity between generated shapes and input text. Among existing methods, the combination of Vector Quantized-Variational AutoEncoder (VQ-VAE) [59] and auto-regressive transformers has emerged as a practical framework for text-to-3D generation [14, 73]. By mapping continuous geometric latent spaces into a discrete token, it reformulates 3D generation as a sequence modeling task, thereby leveraging the scaling potential of transformers.

However, an often overlooked issue is that the quantization process often acts as a filter, where structural topologies are collapsed into indices, making it difficult for the subsequent auto-regressive model to reconstruct fine-grained geometric details from a fragmented latent space. These approaches often suffer from excessive information compression and structural misalignment during encoding and quantization, degrading geometric coherence and limiting the ability of discrete tokens to capture fine-grained, text-specified details. Furthermore, the conventional two-stage paradigm creates a modality gap between representation learning and generative modeling. Since the auto-regressive transformer is optimized solely to minimize cross-entropy in the discrete token space, it remains ‘blind’ to the visual outcome. Consequently, even a high-likelihood token sequence can result in an incoherent shape.

To address these issues, we propose View-aware Auto-Regressive 3D (VAR-3D), a unified framework for text-to-3D generation. First, we introduce a view-aware 3D VQ-VAE that captures complex geometric information, enabling its quantized tokens to better represent object features and improving data reconstruction quality. Second, we further adopt a visual supervision training paradigm that aligns discrete sequence modeling with rendering-supervised, promoting geometric coherence and text-shape alignment. Extensive experiments validate the effectiveness of VAR-3D across multiple evaluation metrics. Our key technical contributions are summarized as follows:

- We design a view-aware 3D VQ-VAE that effectively encodes intricate geometric structures, allowing its discrete tokens to more accurately represent object features and enhance reconstruction fidelity.
- We introduce a rendering-supervised training strategy that bridges the gap between discrete token prediction and visual reconstruction, effectively mitigating the representation-generation mismatch in text-to-3D tasks.

\*Corresponding author.

- Experiments demonstrate that VAR-3D outperforms existing approaches in text-guided 3D synthesis, delivering superior visual fidelity and geometric coherence.

## 2 Related Works

### 2.1 3D Representation and Tokenization

The effectiveness of 3D generative modeling largely depends on the underlying 3D data representation, which directly affects the fidelity, efficiency, and scalability of the generation process. Variational AutoEncoder (VAE) [28] and their discrete variant, VQ-VAE [59], provide an effective framework for compressing high dimensional 3D data into compact latent spaces. Recent large-scale 3D generation methods [29, 67, 71] have further adapted continuous VAE representations to enable diffusion-based priors.

However, continuous latents often exhibit a trade-off between reconstruction fidelity and generative stability when used for powerful generative models. Discrete tokenization alleviates this issue by constraining the latent space and simplifying sequence modeling. VQ-VAE achieves this through a learnable codebook that discretizes continuous features, and has shown strong performance in generative tasks such as text-to-image synthesis [43] and other cross-modal applications [3]. VQ-GAN [21] further improves perceptual quality through adversarial training. Extending vector quantization to 3D remains non-trivial due to the view-dependent and multi-view consistent nature of 3D objects. Existing methods often employ view-agnostic quantization, which may discard important geometric and structural information. These limitations suggest that effective 3D discrete representations should explicitly account for cross-view interactions and hierarchical geometric information.

### 2.2 Paradigms in Text-to-3D Generation

The generation of text into 3D has gone through several different stages of development, transitioning from optimization-based methods to feed-forward generative frameworks. Early Score Distillation Sampling (SDS) approaches [11, 15, 39, 54, 64] synthesize 3D content by distilling priors from pretrained 2D diffusion models. Although these methods are effective, they are limited by high computational cost, the “Janus” (multi-face) problem, and visual over-saturation, which restrict their scalability and stability in practice.

To improve efficiency, subsequent works [35, 36, 46, 47, 65] adopt two-stage pipelines that first generate consistent multi-view images, followed by fast 3D reconstruction [25, 53, 68]. Although significantly faster, these approaches remain constrained by the view-consistency of 2D generators, often leading to geometric artifacts such as floaters and fragmented structures. More recently, native 3D generative models [29, 30, 33, 58, 61, 70, 71] have emerged to directly model 3D distributions. Most existing methods in this category are based on diffusion formulations, which achieve high-quality generation but rely on slow iterative denoising processes. In parallel, auto-regressive models [14, 66, 73] explore sequential or hierarchical token prediction for 3D generation. However, compared to diffusion-based methods, autoregressive models have been relatively less explored in the field of text-to-3D generation. Our VAR-3D further explores the potential of autoregressive models in the field of 3D generation.

### 2.3 Generative Auto-Regressive Models

Auto-regressive (AR) transformers have become a prominent paradigm for visual generation by modeling images or shapes as sequences of discrete tokens. Early works such as PixelCNN [45] and VQ-GAN demonstrated that learning conditional distributions over visual tokens can produce high-quality results with strong global coherence. To alleviate the sequential bottleneck and improve scalability, subsequent studies have explored more efficient tokenization and generation strategies. For example, RQ-VAE [31] employs residual quantization to capture fine-grained details, while the visual auto-regressive framework [55] reformulates next-token prediction into next-scale prediction, thereby achieving improved visual fidelity and accelerating sampling speed.

However, extending these successful approaches [8, 9, 32, 51] to text-to-3D generation remains challenging. Existing 3D autoregressive methods [12, 48, 63], including those based on mesh tokenization, typically suffer from slow generation speed and insufficient robustness when handling geometric shapes. Furthermore, the widely adopted two-stage training paradigm, which separately optimizes the VQ-VAE and the AR transformer, introduces a mismatch between representation learning and sequence modeling. This discrepancy restricts the transformer’s ability to recover information lost during quantization, particularly for fine-grained text–shape alignment, highlighting the need for more coupled representation and training strategies in 3D auto-regressive modeling.

## 3 Methodology

As illustrated in Figure 1, our framework consists of two primary components: a 3D VQ-VAE and a VAR model. In the first stage, the 3D VQ-VAE encodes 3D models into quantized triplane features, which are then represented as discrete multi-scale tokens. In the second stage, the auto-regressive model performs next-scale prediction conditioned on text prompts. In addition to the standard cross-entropy loss, we introduce rendering supervision. Specifically, the predicted tokens are reconstructed by 3D VQ-VAE decoder into 3D models to generate rendered images, which are used to provide additional geometric and visual constraints during training.

### 3.1 3D VQ-VAE

As shown in prior work [6, 9, 29, 44], high-quality visual generation relies on learning a compact and expressive latent space, typically achieved by a carefully designed variational autoencoder. Then, we introduce a 3D VQ-VAE that maps a 3D object into a discrete latent representation for sequence modeling under textual conditions.

**Encoder.** As illustrated in Figure 1, given a 3D object, we first render a set of multi-view RGB-D images, denoted as  $S$ , where  $S = \{s_1, s_2, \dots, s_i\}$ . For each rendering  $s_i = (I, D, C)$ ,  $I \in \mathbb{R}^{H \times W \times 3}$  represents the RGB image,  $D \in \mathbb{R}^{H \times W}$  represents the depth map, and  $C$  represents the corresponding camera parameters. To be compatible with both RGB images and depth maps, we transform the camera parameters  $C$  into Plücker coordinates [49] to obtain  $P \in \mathbb{R}^{H \times W \times 6}$ . In this way, we obtain  $s'_i = (I, D, P) \in \mathbb{R}^{H \times W \times (3+1+6)}$  by a concatenation operation.

To encode our input  $s'$ , we use a multi-view convolutional encoder [14, 47, 53]. For effective feature integration, we preserve

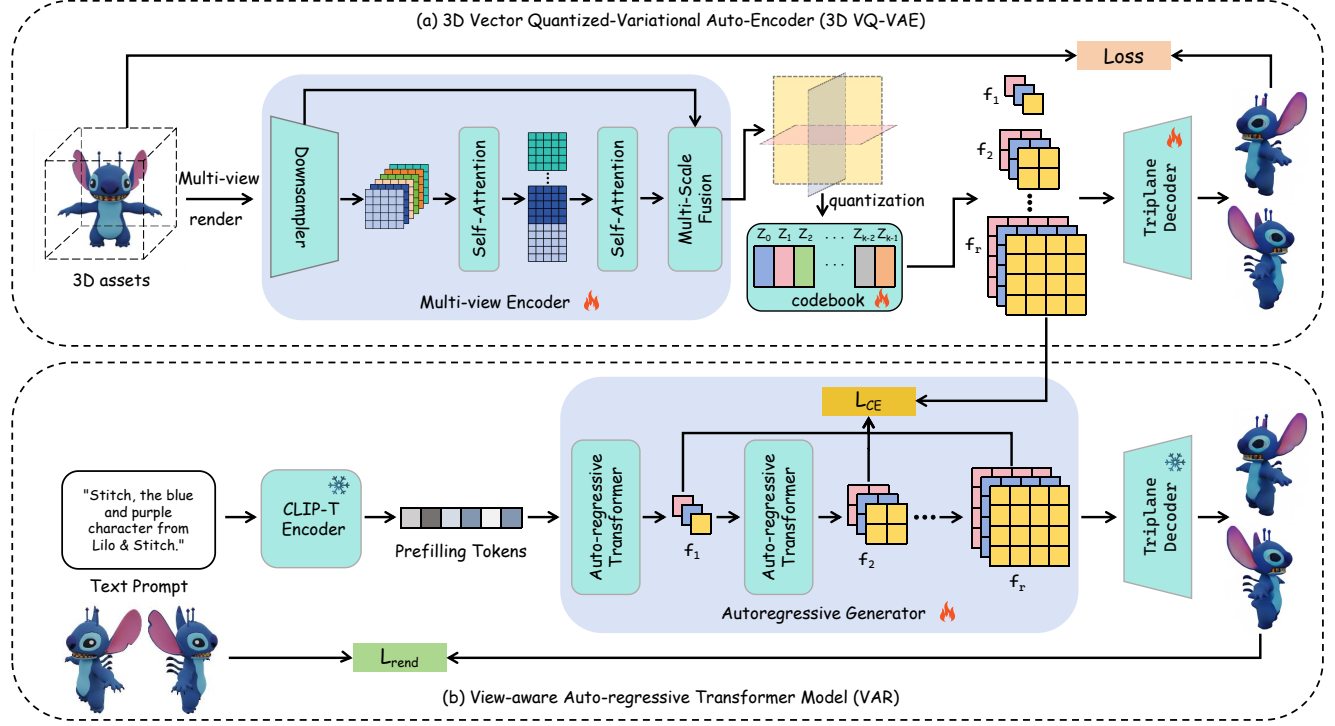


Figure 1: Overall architecture of the proposed VAR-3D framework. (a) 3D VQ-VAE: Multi-view renderings obtained from the 3D asset are encoded with dual self-attention to enhance feature interaction across views. Subsequently, the multi-view features are fused with multi-scale features from the downsampling stage and quantized to obtain latent triplane features  $F = \{f_1, \dots, f_r\}$ , which are decoded to reconstruct the 3D asset by a triplane decoder. (b) VAR model: In text-to-3D generation, the text is encoded into text features by CLIP-T. These text features are used as prefilling tokens for text conditional generation. Then the token sequence is progressively predicted across scales, and triplane features are synthesized via a codebook lookup to generate the 3D asset. Besides, a frozen triplane decoder provides visual supervision during training.

view-aware interaction mechanism during the encode process. Specifically, we utilize the downsampling result  $H = \{h_i\}_{i=1}^6$  and apply self-attention mechanism on each view  $h_i$  to capture details:

$$h_i = \text{SelfAttn}(h_i). \quad (1)$$

Moreover, in order to allow one perspective to perceive other perspectives, we employ a cross-view attention mechanism to model dependencies between different perspectives. Specifically, we concatenate the multi-view features into a unified sequence and process them through a self-attention layer:

$$H' = \text{SelfAttn}(\text{Concat}(H)), \quad (2)$$

this mechanism ensures a comprehensive representation of the 3D structure by aggregating information across all available views.

To mitigate the loss of geometric awareness caused by feature compression during downsampling, we propose a multi-scale feature fusion strategy. We do not rely solely on the final bottleneck layer. Instead, we integrate hierarchical features  $M$  from the last three downsampling layers into the latent representation  $H''$ :

$$H'' = \text{Multi-scaleFusion}(H', M), \quad (3)$$

this multi-level integration effectively preserves both global structure and geometric details. Specifically, we uniformly interpolate the features of each layer of the hierarchical representation  $M$  to match the scale of the latent representation  $H'$ , and then aggregate them through summation. After this, we obtained the latent triplane [14, 29, 67] features  $f \in \mathbb{R}^{h \times w \times 3 \times d}$ , where  $h$  and  $w$  represent the height and width of the triplane feature map, respectively, and  $d$  represents the number of latent channels.

**Quantizer.** We use the embedding vector  $z_q$  from a learnable discrete codebook  $Z = \{z_v\}_{v=1}^V \in \mathbb{R}^{d_q}$  to represent the continuous triplane features. Where  $V$  is the size of the codebook. Specifically, we first need to interpolate the latent triplane features  $f$  to obtain features maps  $F = \{f_{r_1}, f_{r_2}, \dots, f_{r_k}\}$  at different scales  $R = (r_1, r_2, \dots, r_k)$ , which contributes to a progressive and coherent multi-scale representation. To ensure consistency across scales, we employ a shared codebook  $Z$ . Then, we quantize the features  $f_{r_i} \in \mathbb{R}^{(h_{r_i} \times w_{r_i} \times 3) \times d_q}$  at each scale to find the closest codebook entry  $z_q$ , as follows:

$$z_q := (\arg \min_{z_v \in Z} \|f_{r_i} - z_v\|) \in \mathbb{R}^{(h_{r_i} \times w_{r_i} \times 3) \times d_q}. \quad (4)$$

**Decoder.** Following previous works [14, 67], our decoder  $D$  transforms discrete-scale triplanes into a triplane representation. The process begins by converting the discrete-scale tokens into latent features. Next, we perform scale unification to align these features into a consistent space. This results in a unified triplane feature, which is then processed by an upsample to generate the final triplane representation. Finally, we render multiple views from this triplane to calculate the reconstruction loss.

**Training Objective.** To achieve a stable optimization process while preserving high-fidelity geometry and appearance for mesh extraction, we adopt a hybrid training objective that jointly supervises volumetric rendering, discrete latent quantization, and perceptual realism. Specifically, the loss function is defined as:

$$L = \lambda_{\text{render}} L_{\text{render}} + \lambda_{\text{VQ}} L_{\text{VQ}} + \lambda_{\text{GAN}} L_{\text{GAN}}, \quad (5)$$

where each term is weighted by a corresponding coefficient to balance its contribution during training.

**Rendering Loss.** The rendering loss  $L_{\text{render}}$  enforces consistency between the rendered outputs and the ground-truth RGB-D observations, including object silhouettes. To comprehensively capture both low-level reconstruction accuracy and perceptual similarity, we combine pixel-wise and perceptual metrics:

$$L_{\text{render}} = \lambda_{\text{MAE}} L_{\text{MAE}} + \lambda_{\text{SSIM}} L_{\text{SSIM}} + \lambda_{\text{LPIPS}} L_{\text{LPIPS}}, \quad (6)$$

where Mean Absolute Error (MAE) penalizes pixel-wise discrepancies, Structural Similarity Index Measure (SSIM) preserves structural coherence, and Learned Perceptual Image Patch Similarity (LPIPS) [58] encourages perceptual alignment in a learned feature space.

**Vector Quantization Loss.** To learn compact and discrete latent representations, we employ the vector quantization loss  $L_{\text{VQ}}$  [59] to supervise the update of the codebook. This loss function aims to minimize the difference between the encoder features and their corresponding quantized embeddings:

$$L_{\text{VQ}} = \sum_{r_i} (|\text{sg}[f_{r_i}] - z_q^{r_i}| + \beta |f_{r_i} - \text{sg}[z_q^{r_i}]|), \quad (7)$$

where  $f_{r_i}$  denotes the encoder feature at region  $r_i$ ,  $\beta$  is the ratio between the two losses,  $z_q^{r_i}$  represents the selected codebook vector, and  $\text{sg}[\cdot]$  is the stop-gradient operator [4]. The first term is used to update the codebook, while the second term, the commitment loss, regularizes the encoder output to close the quantized embeddings, thus stabilizing the learning process of the discrete latent space.

**Adversarial Loss.** We incorporate an adversarial loss  $L_{\text{GAN}}$  [22] to improve perceptual realism. The critic  $D$  is trained with WGAN-GP; the loss for the critic (discriminator) is:

$$L_D = \mathbb{E}_{\tilde{x} \sim p_g} [D(\tilde{x})] - \mathbb{E}_{x \sim p_r} [D(x)] + \lambda \mathbb{E}_{\tilde{x} \sim p_{\tilde{x}}} [(\|\nabla_{\tilde{x}} D(\tilde{x})\|_2 - 1)^2], \quad (8)$$

where  $x \sim p_r$  and  $\tilde{x} \sim p_g$  denote ground-truth and generated samples respectively. The generator minimizes the objective:

$$L_{\text{GAN}} = -\mathbb{E}_{z \sim p_z} [D(G(z))], \quad (9)$$

with  $G(z)$  producing generated samples from latent codes  $z \sim p_z$ .

### 3.2 View-aware Auto-regressive Model

The discrete token maps obtained from the first stage are used to train a text-conditioned autoregressive shape generation model. Our model follows a next-scale prediction strategy [14, 55, 74],

generating a sequence of token maps  $\{f_{r_1}, f_{r_2}, \dots, f_{r_k}\}$  progressively guided by input the prefilling tokens, which is generated from text.

**Sequence Construction.** Initially, 3D shapes are encoded into discrete triplane features using a 3D VQ-VAE. Each feature is represented as an index from a learned codebook. These indices are then serialized into a multi-scale sequence. Within the sequence, indices of each plane are arranged in raster-scan order. To preserve spatial correlation across planes, indices corresponding to the same spatial location in the three planes are placed consecutively.

**Text-Conditional Generation.** Our approach differs from feed-forward 3D reconstruction methods [25, 53], which directly map an input image to a 3D representation. Instead, we focus on generating 3D shapes conditioned on text prompts. Text embeddings are extracted using a CLIP-T [41] ViT-L encoder and injected into the autoregressive model via cross-attention. This allows semantic information from text to guide the generation process. To provide global semantic context, we use the pooled CLIP text embedding as an initial conditioning token for the generation sequence.

**Autoregressive Generator.** Generation proceeds from an initial low-resolution token map to progressively higher resolutions. The final token map  $f_{r_k}$  matches the resolution of the original feature map. We implement the generator as GPT-2 style decoder-only Transformer [7]. The autoregressive likelihood is formulated as:

$$p(f_{r_1}, f_{r_2}, \dots, f_{r_k}) = \prod_{i=1}^k p(f_{r_i} | f_{<r_i}), \quad (10)$$

where  $f_{<r_i}$  denotes all preceding scales. Tokens at each scale are predicted in parallel, while the model conditions on previous scales. For text-conditional synthesis, a text embedding  $c$  acts as both the start token and a conditioning factor via Adaptive Layer Normalization (AdaLN) [38]. Queries and keys are normalized to unit length before attention to improve training stability. The model is trained with a token-level cross-entropy loss:

$$L_{\text{CE}} = -\frac{1}{K} \sum_{i=1}^K \log p(f_{r_i} | f_{<r_i}, c), \quad (11)$$

which encourages the model to assign high probabilities to the correct token maps and ensures accurate generation across all scales.

**Rendering-Based Structural Supervision.** While  $L_{\text{CE}}$  ensures token-wise prediction accuracy, it does not explicitly enforce global geometric continuity or fine-grained structural details. To bridge this gap, we introduce a differentiable rendering-based supervision pipeline. However, the standard discrete sampling (e.g., *argmax*) of AR tokens is non-differentiable, which prevents gradients from the rendering loss from backpropagating to the AR model. To resolve this, we employ the Gumbel-Softmax Straight-Through Estimator (STE) to obtain a differentiable approximation of the discrete token map. Specifically, given the predicted logits  $L$ , we compute the differentiable one-hot representation  $f_z$ :

$$f_z = \text{Gumbel-Softmax}(L, \tau, \text{hard=True}), \quad (12)$$

where  $\tau$  is the temperature. The forward pass uses discrete selections to maintain fidelity, while the backward pass uses continuous relaxations to propagate gradients. These tokens are then mapped



**Figure 2: Visual comparison of 3D reconstruction.** We present reconstruction 3D objects generated by our 3D VQ-VAE displaying two views of each sample. Compared to the baseline methods, our approach consistently yields better quality regarding geometry, texture. Furthermore, our method also demonstrates better performance in terms of multi-view consistency.

to the codebook and reshaped into a multi-scale 3D triplane representation. The reconstructed triplanes are then projected into 2D images  $I_{\text{pred}}$  from multiple views using a differentiable renderer  $\mathcal{R}$ . Ground-truth images  $I_{\text{gt}}$  are rendered from the original 3D shapes under the same camera settings. We define the multi-view rendering loss as a weighted combination of  $\ell_1$  and  $\ell_2$  losses:

$$L_{\text{rend}} = \lambda_1 |I_{\text{pred}} - I_{\text{gt}}|_1 + \lambda_2 |I_{\text{pred}} - I_{\text{gt}}|_2^2, \quad (13)$$

where  $\lambda_1$  and  $\lambda_2$  are used to balance the contributions of each loss.

**Training Objective.** The total loss used to train the autoregressive model combines token-level supervision and rendering-based visual supervision:

$$L_{\text{total}} = L_{\text{CE}} + \gamma L_{\text{rend}}, \quad (14)$$

where  $\gamma$  balances the two training objectives. The cross-entropy loss enforces accurate token prediction, while the rendering-based loss provides additional visual and geometric guidance.

## 4 Experiments

### 4.1 Experiment Setup

**Datasets.** We train our model on the G-Objaverse dataset [18, 19, 40], which contains RGB images, normal maps, depth maps, and

corresponding camera poses. The dataset contains approximately 280K data spanning 10 general categories, including Human-Shape, Animals, Daily-Used, Furniture, Buildings & Outdoor, Transportation, Plants, Food, Electronics, and Poor-quality. Following works [14, 29], we adopt a high-quality subset consisting of around 100K 3D assets for training. For text-conditioned generation, we use the captions as text prompts, which is provided by 3D-Topia [16, 24].

**Metrics.** We compare the novel views rendered from the synthesized 3D asset with the ground truth views based on a set of common metrics, including Peak Signal-to-Noise Ratio (PSNR), LPIPS [72], SSIM [62]. Additionally, we utilize Fréchet Inception Distance(FID) [23], and Kernel Inception Distance(KID) [5] to assess the overall distribution quality between the generated output and the ground truth, and use CLIP-T scores [42] to evaluate the consistency between the generated results and the input text prompts.

**Implementation Details.** In our 3D VQ-VAE training stage, we use input images with a resolution of  $H = W = 256$ . The model takes 6 rendered views ( $i = 6$ ) as multi-view inputs. We follow [14] by applying the feature map  $R$  is quantized in a multi-scale manner across ten scales. We set the codebook size  $V$  to 16,384 and the codebook channel dimension  $d_q$  to 8. The hyperparameters in

**Table 1: Quantitative evaluation of text conditioned 3D generation.** As shown below, the proposed method demonstrates strong performance across all metrics. KID scores are scaled by  $10^2$ ,  $\uparrow$ : the higher value, the better performance,  $\downarrow$ : the lower the better.

Method	PSNR $\uparrow$	SSIM $\uparrow$	CLIP-T $\uparrow$	FID $\downarrow$	KID(%) $\downarrow$	LPIPS $\downarrow$
Shape-E [27]	12.13	0.753	26.98	56.99	1.219	0.306
LGM [53]	14.94	0.811	25.73	41.83	0.882	0.236
LN3Diff [29]	15.70	0.767	25.84	61.16	1.523	0.292
SAR3D [14]	18.31	0.832	<b>27.66</b>	36.84	0.559	0.199
<b>Ours</b>	<b>18.52</b>	<b>0.840</b>	27.42	<b>32.74</b>	<b>0.396</b>	<b>0.176</b>

Eqn.(5) are set as  $\lambda_{\text{render}} = 1$ ,  $\lambda_{VQ} = 1$  and  $\lambda_{\text{GAN}} = 0.025$ , and Eqn.(6) are set as  $\lambda_{\text{MAE}} = 1$ ,  $\lambda_{\text{SSIM}} = 0.2$  and  $\lambda_{\text{LPIPS}} = 0.8$ . We use a constant learning rate for training, initialized to  $1e-4$  and adopt the AdamW optimizer [42] to train the 3D VQ-VAE.

To train our VAR model at second stage, our architecture is based on visual auto-regressive framework [55], adding plane positional encoding for each plane, which has 16 transformer blocks with 16 heads. We use the AdamW optimizer set the learning rate of  $1e-4$ , with a linear decaying learning rate schedule for training. At the same time, for rendering-based structural supervision, we randomly select a view rendering from 6 views as supervision and we use frozen triplane decoder to reconstruct pred model. The hyperparameters in Eqn.(13) and Eqn.(14) are set as  $\lambda_1 = 0.2$ ,  $\lambda_2 = 8$  and  $\gamma = 0.1$ . We set the batch size to 32 for 3D VQ-VAE with 100K iterations and to 16 for VAR model with 100 epochs. The entire training procedure was performed using 2 NVIDIA RTX 4090 GPUs.

## 4.2 Reconstruction Result

We first compare the reconstruction fidelity of our method with other triplane-based approaches. LN3Diff [29] uses a continuous latent triplane representation with VAE, whereas SAR3D [14] adopts a discrete representation based on VQ-VAE.

For appearance evaluation, we compute the PSNR and SSIM between rendered reconstructions and ground-truth images. We further assess distribution-level quality using FID and KID. As shown in Table 2, our method consistently outperforms all baselines across all metrics. Specifically, it achieves a PSNR of 28.97 and an SSIM of 0.938, surpassing LN3Diff (25.63/0.894) and SAR3D (28.04/0.927). At the distribution level, our method attains lower FID and KID scores (30.50 and 0.140), compared to 35.92/0.161 for SAR3D and 63.35/1.044 for LN3Diff, indicating our model better alignment with the ground truth data distribution.

Qualitative comparisons in Figure 2 further validate these results. Our method produces reconstructions with more faithful appearances and finer geometric details, closely matching the ground-truth 3D models. In contrast, while LN3Diff [29] preserves some details of complex objects, it suffers from shortcomings in the appearance of object and geometric accuracy; while SAR3D [14] generates relatively accurate geometric shapes, it suffers from viewpoint inconsistency issues, thus reducing the overall reconstruction quality.

## 4.3 Generation Result

In this section, we first report quantitative comparisons with existing methods using standard evaluation metrics. Complementary

**Table 2: Quantitative comparison of 3D reconstruction.** We evaluate the reconstruction fidelity based on different methods using latent triplane representation.

Method	PSNR $\uparrow$	SSIM $\uparrow$	FID $\downarrow$	KID(%) $\downarrow$
LN3Diff [29]	25.63	0.894	63.35	1.044
SAR3D [14]	28.04	0.927	35.92	0.161
<b>Ours</b>	<b>28.97</b>	<b>0.938</b>	<b>30.50</b>	<b>0.140</b>

qualitative results are provided to illustrate the visual quality, structural coherence, and consistency of the generated 3D content.

**Quantitative Evaluation.** We performed a quantitative comparison of 500 test samples from the Objaverse dataset [18, 19]. For each 3D asset, a corresponding text prompt is generated using 3D-Topia, and all methods are evaluated by rendering the generated shapes from 6 views at a resolution of  $256 \times 256$ .

As reported in Table 1, our method demonstrates strong and consistent performance across both reconstruction and perceptual metrics. It achieves the highest PSNR (18.52) and SSIM (0.840) among all methods, indicating improved reconstruction fidelity and more accurate geometric recovery. Although SAR3D attains the best CLIP-T score (27.66), our method achieves a comparable CLIP-T of 27.42, suggesting similarly strong text-3D semantic alignment. In addition, our approach outperforms prior methods in terms of perceptual quality and distribution-level similarity, achieving the lowest FID (32.74), KID (0.396), and LPIPS (0.176). These results indicate that our method produces 3D assets that are closer to the ground-truth distribution while maintaining high perceptual realism, leading to a favorable trade-off between reconstruction accuracy, perceptual quality, and text-conditioned alignment.

**Qualitative Evaluation.** Figure 3 presents a qualitative evaluation of our method against representative text-conditioned 3D generation approaches, including 2D-assisted methods LGM [53], native 3D diffusion models: Shape-E [27], LN3Diff, and autoregressive 3D generation methods SAR3D. Meanwhile, it also proved that our quantitative assessment was correct and effective.

As shown in Figure 3, our method consistently outperforms previous approaches by producing results with more vivid appearances, finer geometric details, and more accurate alignment with the provided text prompts. In contrast, existing methods suffer from varying degrees of quality degradation in both geometry and semantic consistency. Specifically, native 3D diffusion methods tend



**Figure 3: Qualitative comparison of text-conditioned 3D generation.** We present text-to-3D generation results for objects generated by our method, displaying two views of each sample. Compared to the baseline methods, our approach consistently yields better quality regarding geometry, texture, and text-3D alignment.

**Table 3: Ablation study of different components in our 3D VQ-VAE model. We ablate the design of our model architecture. Each component contributes to consistent gains in reconstruction performance and improves the modeling capacity.**

Setting	PSNR $\uparrow$	FID $\downarrow$	KID(%) $\downarrow$
base	28.42	34.72	0.165
w/ view-aware interaction	28.57	33.35	0.151
w/ multi-scale fusion	28.68	32.00	0.150
full	28.97	30.50	0.140

to generate objects that lack distinctive features and fine-grained geometric details, largely due to the limited reconstruction accuracy of their latent representations. For instance, LN3Diff fails to faithfully capture structural details in the example prompted by *"A small blue and white ceramic jar with a lid."*, resulting in visible geometric artifacts. Although LGM is able to generate visually

plausible objects, it often struggles to produce reasonable and coherent geometric shapes, which can be attributed to the inherent limitations of its 3D Gaussian representation. Furthermore, while SAR3D can synthesize images with relatively good visual quality, its results may not always align well with the given text descriptions. As illustrated by the prompt *"Yellow leather chair with wooden legs."* SAR3D fails to correctly capture the *"wooden legs"* attribute, indicating insufficient text-geometry understanding.

#### 4.4 Ablation Studies

We conduct ablation studies to analyze the contributions of key components in our framework. Specifically, we evaluate the effects of the multi-scale feature fusion and view-aware interaction modules on the 3D VQ-VAE, examine the influence of different codebook sizes during training, and assess the impact of vision-based supervision strategy on the autoregressive model.

**3D VQ-VAE Ablations.** We assess the effectiveness of the proposed view-aware interaction and multi-scale fusion modules, as summarized in Table 3. Specifically, disabling multi-scale fusion



**Figure 4: Visual comparison of our 3D VQ-VAE ablation experiments on the effectiveness of our components**

**Table 4: Ablation study of different codebook size in our 3D VQ-VAE model. Larger codebooks increase shape diversity and enhance reconstruction performance.**

Codebook Size	PSNR $\uparrow$	SSIM $\uparrow$	LPIPS $\downarrow$
4096	28.58	0.932	0.069
8192	28.87	0.936	0.065
16384	28.97	0.938	0.063

reduces the PSNR from 28.97 to 28.57 and increases the FID to 33.35 and the KID to 0.151, while removing the view-aware interaction module also results in lower PSNR and higher FID/KID scores. As shown in Table 4, changing the codebook size in the 3D VQ-VAE significantly affects model performance. A larger codebook yields better reconstruction results, indicating that the model is better able to capture shape diversity and preserve a wider variety of shapes.

Qualitative results in Figure 4 provide further evidence supporting these findings. When the proposed modules are removed, the model exhibits noticeable geometric distortions and struggles to maintain fine-grained details, particularly under the interference introduced by multiple views. In contrast, incorporating the proposed modules substantially improves reconstruction quality, leading to better preservation of structural coherence and sharper local details across views, resulting in inconsistent geometry across views.

**Training Objective Ablations.** We conduct ablation studies on the training objectives to evaluate the impact of the proposed rendering-based visual loss ( $L_{\text{rend}}$ ) in the second-stage autoregressive model. To assess the contribution of  $L_{\text{rend}}$ , we adopt a removal-based ablation protocol. Specifically, we fine-tune the autoregressive transformer under different loss configurations using a reduced subset of 20k training samples for 20 epochs. The considered settings include retaining the full objective ( $L_{\text{CE}} + L_{\text{rend}}$ ) and removing the rendering-based loss, i.e., optimizing with  $L_{\text{CE}}$  only.

**Table 5: Ablation study of training objectives at second stage. Introducing visual supervision,  $L_{\text{rend}}$  improves distribution-level similarity, as reflected by lower FID and KID.**

Training Objective	$L_{\text{CE}}$	$L_{\text{CE}} + L_{\text{rend}}$
CLIP-T $\uparrow$	27.26	27.17
FID $\downarrow$	42.61	41.26
KID(%) $\downarrow$	0.701	0.655

This allows us to isolate the effect of the rendering-based supervision while keeping the model initialization, tokenizer, and token distribution fixed, and focuses on evaluating the performance degradation caused by removing  $L_{\text{rend}}$ . As shown in Table 5, removing the rendering-based loss leads to a noticeable degradation in FID and KID, indicating that  $L_{\text{rend}}$  plays an important role in maintaining visual fidelity and distribution-level quality. Meanwhile, the CLIP-T score remains largely stable with only a decrease, while FID and KID show clear improvements, indicating that the rendering-based loss enhances distribution-level visual quality without compromising text-3D semantic alignment. These results demonstrate that the rendering-based loss effectively complements cross-entropy, enabling better learning of 3D discrete representations.

## 5 Limitations

Although VAR-3D produces high-quality 3D objects, it still relies on a two-stage training pipeline rather than a fully end-to-end design. Future work may explore unified end-to-end 3D generation. Moreover, the current framework only supports text-conditioned generation and does not handle image or multimodal inputs. In addition, the quality of geometry and texture is constrained by volume rendering, and adopting more efficient 3D representations [26] could further improve results. Finally, due to limited computational resources, we did not further explore the impact of visual supervision on the model or the scalability of our method. Nevertheless, prior work on 2D scaling laws in visual auto-regressive frameworks [55] indicates its could potentially extend to larger-scale 3D content.

## 6 Conclusion

In this work, we presented VAR-3D, a novel framework that advances 3D object generation by text-conditioned. By introducing the view-aware 3D VQ-VAE, we mitigated compression losses and view inconsistencies during the encoding 3D objects, thereby achieving high-quality 3D reconstruction and representation. Furthermore, we use the frozen 3D VQ-VAE decoder as a visual reconstruction supervision during the second stage of the training process, ensuring that the generated 3D objects conform not only to the latent triplane distribution but also to the vision-based distribution. Both quantitative and qualitative results demonstrate the effectiveness of our method, highlighting the potential of auto-regressive 3D generation. Future research could further explore end-to-end training and extend it to a wider range of 3D content, multimodal-condition generation and understanding challenges.

## References

[1] Josh Achiam, Steven Adler, Sandhini Agarwal, Lama Ahmad, Ilge Akkaya, Florencia Leoni Aleman, Diogo Almeida, Janko Altenschmidt, Sam Altman, Shyamal Anadkat, et al. 2023. Gpt-4 technical report. *arXiv preprint arXiv:2303.08774* (2023).

[2] Jean-Baptiste Alayrac, Jeff Donahue, Pauline Luc, Antoine Miech, Iain Barr, Yana Hasson, Karel Lenc, Arthur Mensch, Katherine Millican, Malcolm Reynolds, et al. 2022. Flamingo: a visual language model for few-shot learning. 35 (2022), 23716–23736.

[3] Tenglong Ao, Qingzhe Gao, Yuke Lou, Baoquan Chen, and Libin Liu. 2022. Rhythmic gesticulator: Rhythm-aware co-speech gesture synthesis with hierarchical neural embeddings. *ACM Transactions on Graphics (TOG)* 41, 6 (2022), 1–19.

[4] Yoshua Bengio, Nicholas Léonard, and Aaron Courville. 2013. Estimating or propagating gradients through stochastic neurons for conditional computation. *arXiv preprint arXiv:1308.3432* (2013).

[5] Mikołaj Bińkowski, Danica J Sutherland, Michael Arbel, and Arthur Gretton. 2018. Demystifying MMD GANs.

[6] Tim Brooks, Bill Peebles, Connor Holmes, Will DePue, Yufei Guo, Li Jing, David Schnurr, Joe Taylor, Troy Luhman, Eric Luhman, et al. 2024. Video generation models as world simulators. *OpenAI Blog* 1 (2024), 8.

[7] Tom Brown, Benjamin Mann, Nick Ryder, Melanie Subbiah, Jared D Kaplan, Prafulla Dhariwal, Arvind Neelakantan, Pranav Shyam, Girish Sastry, Amanda Askell, et al. 2020. Language models are few-shot learners. 33 (2020), 1877–1901.

[8] Huiwei Chang, Han Zhang, Jarred Barber, AJ Maschinot, Jose Lezama, Lu Jiang, Ming-Hsuan Yang, Kevin Murphy, William T. Freeman, Michael Rubinstein, Yuanzhen Li, and Dilip Krishnan. 2023. Muse: Text-To-Image Generation via Masked Generative Transformers. *arXiv preprint arXiv:2301.00704* (2023).

[9] Huiwei Chang, Han Zhang, Lu Jiang, Ce Liu, and William T. Freeman. 2022. MaskGIT: Masked Generative Image Transformer. In *CVPR*.

[10] Jinnan Chen, Chen Li, Jianfeng Zhang, Lingting Zhu, Buzhen Huang, Hanlin Chen, and Gim Hee Lee. 2024. Generalizable Human Gaussians from Single-View Image. *arXiv preprint arXiv:2406.06050* (2024).

[11] Rui Chen, Yongwei Chen, Ningxin Jiao, and Kui Jia. 2023. Fantasia3d: Disentangling geometry and appearance for high-quality text-to-3d content creation. 22246–22256.

[12] Sijin Chen, Xin Chen, Anqi Pang, Xianfang Zeng, Wei Cheng, Yijun Fu, Fukun Yin, Yanru Wang, Zhibin Wang, Chi Zhang, et al. 2024. MeshXL: Neural Coordinate Field for Generative 3D Foundation Models. *arXiv preprint arXiv:2405.20853* (2024).

[13] Yiwen Chen, Tong He, Di Huang, Weicai Ye, Sijin Chen, Jiaxiang Tang, Xin Chen, Zhonghang Cai, Lei Yang, Gang Yu, Guosheng Lin, and Chi Zhang. 2025. MeshAnything: Artist-Created Mesh Generation with Autoregressive Transformers.

[14] Yongwei Chen, Yushi Lan, Shangchen Zhou, Tengfei Wang, and Xingang Pan. 2025. SAR3D: Autoregressive 3D Object Generation and Understanding via Multi-scale 3D VQVAE. (2025).

[15] Yongwei Chen, Tengfei Wang, Tong Wu, Xingang Pan, Kui Jia, and Ziwei Liu. 2024. Comboverse: Compositional 3d assets creation using spatially-aware diffusion guidance. Springer, 128–146.

[16] Zhaoxi Chen, Jiaxiang Tang, Yuhao Dong, Ziang Cao, Fangzhou Hong, Yushi Lan, Tengfei Wang, Haozhu Xie, Tong Wu, Shunsuke Saito, et al. 2025. 3dtopia-xl: Scaling high-quality 3d asset generation via primitive diffusion. In *Proceedings of the Computer Vision and Pattern Recognition Conference*. 26576–26586.

[17] Aakanksha Chowdhery, Sharan Narang, Jacob Devlin, Maarten Bosma, Gaurav Mishra, Adam Roberts, Paul Barham, Hyung Won Chung, Charles Sutton, Sebastian Gehrmann, et al. 2023. Palm: Scaling language modeling with pathways. 24, 240 (2023), 1–113.

[18] Matt Deitke, Ruoshi Liu, Matthew Wallingford, Huong Ngo, Oscar Michel, Aditya Kusupati, Alan Fan, Christian Lafforte, Vikram Voleti, Samir Yitzhak Gadre, et al. 2023. Objaverse-xl: A universe of 10m+ 3d objects. 36 (2023), 35799–35813.

[19] Matt Deitke, Dustin Schwenk, Jordi Salvador, Luca Weihs, Oscar Michel, Eli VanderBilt, Ludwig Schmidt, Kiana Ehsani, Aniruddha Kembhavi, and Ali Farhadi. 2023. Objaverse: A universe of annotated 3d objects. 13142–13153.

[20] Danny Driess, Fei Xia, Mehdi SM Sajjadi, Corey Lynch, Aakanksha Chowdhery, Brian Ichter, Ayaan Wahid, Jonathan Tompson, Quan Vuong, Tianhe Yu, et al. 2023. PaLM-E: An Embodied Multimodal Language Model. (2023), 8469–8488.

[21] Patrick Esser, Robin Rombach, and Bjorn Ommer. 2021. Taming transformers for high-resolution image synthesis. In *Proceedings of the IEEE/CVF conference on computer vision and pattern recognition*. 12873–12883.

[22] Ishaan Gulrajani, Faruk Ahmed, Martin Arjovsky, Vincent Dumoulin, and Aaron Courville. 2017. Improved Training of Wasserstein GANs. (2017). *arXiv:1704.00028*

[23] Martin Heusel, Hubert Ramsauer, Thomas Unterthiner, Bernhard Nessler, and Sepp Hochreiter. 2017. Gans trained by a two time-scale update rule converge to a local nash equilibrium. 30 (2017).

[24] Fangzhou Hong, Jiaxiang Tang, Ziang Cao, Min Shi, Tong Wu, Zhaoxi Chen, Tengfei Wang, Liang Pan, Dahu Lin, and Ziwei Liu. 2024. 3DTopia: Large Text-to-3D Generation Model with Hybrid Diffusion Priors. *arXiv preprint arXiv:2403.02234* (2024).

[25] Yicong Hong, Kai Zhang, Jiaxiang Gu, Sai Bi, Yang Zhou, Difan Liu, Feng Liu, Kalyan Sunkavalli, Trung Bui, and Hao Tan. 2024. LRM: Large Reconstruction Model for Single Image to 3D. *arXiv preprint arXiv:2311.04400* (2024).

[26] Binbin Huang, Zehao Yu, Anpei Chen, Andreas Geiger, and Shenghua Gao. 2024. 2d gaussian splatting for geometrically accurate radiance fields. 1–11.

[27] Heewoo Jun and Alex Nichol. 2023. Shap-E: Generating Conditional 3D Implicit Functions. (2023). *arXiv:2305.02463*

[28] Diederik P Kingma. 2013. Auto-encoding variational bayes. *arXiv preprint arXiv:1312.6114* (2013).

[29] Yushi Lan, Fangzhou Hong, Shuai Yang, Shangchen Zhou, Xuyi Meng, Bo Dai, Xingang Pan, and Chen Change Loy. 2024. LN3Diff: Scalable Latent Neural Fields Diffusion for Speedy 3D Generation. (2024).

[30] Yushi Lan, Shangchen Zhou, ZhaoYang Lyu, Fangzhou Hong, Shuai Yang, Bo Dai, Xingang Pan, and Chen Change Loy. 2025. GaussianAnything: Interactive Point Cloud Latent Diffusion for 3D Generation.

[31] Doyup Lee, Chiheon Kim, Saehoon Kim, Minsu Cho, and Wook-Shin Han. 2022. Autoregressive Image Generation using Residual Quantization. In *CVPR*.

[32] Tianhong Li, Yonglong Tian, He Li, Mingyang Deng, and Kaiming He. 2024. Autoregressive Image Generation without Vector Quantization. *arXiv preprint arXiv:2406.11838* (2024).

[33] Weiyu Li, Jiarui Liu, Hongyu Yan, Rui Chen, Yixun Liang, Xuelin Chen, Ping Tan, and Xiaoxiao Long. 2025. CraftsMan: High-fidelity Mesh Generation with 3D Native Generation and Interactive Geometry Refiner.

[34] Yuan Liu, Cheng Lin, Zijiao Zeng, Xiaoxiao Long, Lingjie Liu, Taku Komura, and Wenping Wang. 2023. Syncdreamer: Generating multiview-consistent images from a single-view image. *arXiv preprint arXiv:2309.03453* (2023).

[35] Zexiang Liu, Yangguang Li, Youtian Lin, Xin Yu, Sida Peng, Yan-Pei Cao, Xiaojuan Qi, Xiaoshui Huang, Ding Liang, and Wanli Ouyang. 2025. Unidream: Unifying diffusion priors for relightable text-to-3d generation. In *European Conference on Computer Vision*. Springer, 74–91.

[36] Xiaoxiao Long, Yuan-Chen Guo, Cheng Lin, Yuan Liu, Zhiyang Dou, Lingjie Liu, Yuexin Ma, Song-Hai Zhang, Marc Habermann, Christian Theobalt, et al. 2024. Wonder3d: Single image to 3d using cross-domain diffusion. 9970–9980.

[37] Long Ouyang, Jeffrey Wu, Xu Jiang, Diogo Almeida, Carroll Wainwright, Pamela Mishkin, Chong Zhang, Sandhini Agarwal, Katarina Slama, Alex Ray, et al. 2022. Training language models to follow instructions with human feedback. 35 (2022), 27730–27744.

[38] William Peebles and Saining Xie. 2023. Scalable diffusion models with transformers. 4195–4205.

[39] Ben Poole, Ajay Jain, Jonathan T Barron, and Ben Mildenhall. 2023. DreamFusion: Text-to-3D using 2D Diffusion.

[40] Lingteng Qiu, Guanying Chen, Xiaodong Gu, Qi Zuo, Mutian Xu, Yushuang Wu, Weihao Yuan, Zilong Dong, Liefeng Bo, and Xiaoguang Han. 2024. Richdreamer: A generalizable normal-depth diffusion model for detail richness in text-to-3d. 9914–9925.

[41] Alec Radford, Jong Wook Kim, Chris Hallacy, Aditya Ramesh, Gabriel Goh, Sandhini Agarwal, Girish Sastry, Amanda Askell, Pamela Mishkin, Jack Clark, et al. 2021. Learning transferable visual models from natural language supervision. *arXiv:2112.09747* (2021). PMLR, 8748–8763.

[42] Alec Radford, Jong Wook Kim, Chris Hallacy, Aditya Ramesh, Gabriel Goh, Sandhini Agarwal, Girish Sastry, Amanda Askell, Pamela Mishkin, Jack Clark, et al. 2021. Learning transferable visual models from natural language supervision. In *International conference on machine learning*. PMLR.

[43] Aditya Ramesh, Mikhail Pavlov, Gabriel Goh, Scott Gray, Chelsea Voss, Alec Radford, Mark Chen, and Ilya Sutskever. 2021. Zero-shot text-to-image generation. In *International conference on machine learning*. PMLR, 8821–8831.

[44] Robin Rombach, Andreas Blattmann, Dominik Lorenz, Patrick Esser, and Björn Ommer. 2022. High-resolution image synthesis with latent diffusion models. 10684–10695.

[45] Tim Salimans, Andrej Karpathy, Xi Chen, and Diederik P Kingma. 2017. PixelCNN++: Improving the PixelCNN with Discretized Logistic Mixture Likelihood and Other Modifications.

[46] Ruoxi Shi, Hansheng Chen, Zhuoyang Zhang, Minghua Liu, Chao Xu, Xinyue Wei, Linghao Chen, Chong Zeng, and Hao Su. 2023. Zero23++: a Single Image to Consistent Multi-view Diffusion Base Model. In *arXiv*.

[47] Yichun Shi, Peng Wang, Jianglong Ye, Long Mai, Kejie Li, and Xiao Yang. 2023. MVdream: Multi-view Diffusion for 3D Generation. *arXiv preprint arXiv:2308.16512* (2023).

[48] Yawar Siddiqui, Antonio Alliegro, Alexey Artemov, Tatiana Tommasi, Daniele Sirigatti, Vladislav Rosov, Angela Dai, and Matthias Nießner. 2023. MeshGPT: Generating Triangle Meshes with Decoder-Only Transformers. In *CVPR*.

[49] Vincent Sitzmann, Semon Rezchikov, Bill Freeman, Josh Tenenbaum, and Fredo Durand. 2021. Light field networks: Neural scene representations with single-evaluation rendering. 34 (2021), 19313–19325.

[50] Peize Sun, Yi Jiang, Shoufa Chen, Shilong Zhang, Bingyue Peng, Ping Luo, and Zehuan Yuan. 2024. Autoregressive Model Beats Diffusion: Llama for Scalable

Image Generation. *arXiv preprint arXiv:2406.06525* (2024).

[51] Peize Sun, Yi Jiang, Shoufa Chen, Shilong Zhang, Bingyue Peng, Ping Luo, and Zehuan Yuan. 2024. Autoregressive Model Beats Diffusion: Llama for Scalable Image Generation. *arXiv preprint arXiv:2406.06525* (2024).

[52] Quan Sun, Qiyi Yu, Yufeng Cui, Fan Zhang, Xiaosong Zhang, Yueze Wang, Hongcheng Gao, Jingjing Liu, Tiejun Huang, and Xinlong Wang. 2024. Emu: Generative Pretraining in Multimodality. (2024).

[53] Jiaxiang Tang, Zhaoxi Chen, Xiaokang Chen, Tengfei Wang, Gang Zeng, and Ziwei Liu. 2024. LGM: Large Multi-View Gaussian Model for High-Resolution 3D Content Creation. *arXiv preprint arXiv:2402.05054* (2024).

[54] Junshu Tang, Tengfei Wang, Bo Zhang, Ting Zhang, Ran Yi, Lizhuang Ma, and Dong Chen. 2023. Make-it-3d: High-fidelity 3d creation from a single image with diffusion prior. (2023), 22819–22829.

[55] Keyu Tian, Yi Jiang, Zehuan Yuan, Bingyue Peng, and Liwei Wang. 2024. Visual autoregressive modeling: Scalable image generation via next-scale prediction. 37 (2024), 84839–84865.

[56] Dmitry Tochilkin, David Pankratz, Zexiang Liu, Zixuan Huang, Adam Letts, Yangguang Li, Ding Liang, Christian Laforte, Varun Jampani, and Yan-Pei Cao. 2024. TripoSR: Fast 3D Object Reconstruction from a Single Image. *arXiv preprint arXiv:2403.02151* (2024).

[57] Hugo Touvron, Thibaut Lavrille, Gautier Izacard, Xavier Martinet, Marie-Anne Lachaux, Timothée Lacroix, Baptiste Rozière, Naman Goyal, Eric Hambro, Faisal Azhar, et al. 2023. Llama: Open and efficient foundation language models. *arXiv preprint arXiv:2302.13971* (2023).

[58] Arash Vahdat, Francis Williams, Zan Gojcic, Or Litany, Sanja Fidler, Karsten Kreis, et al. 2022. Lion: Latent point diffusion models for 3d shape generation. 35 (2022), 10021–10039.

[59] Aaron Van Den Oord, Oriol Vinyals, et al. 2017. Neural discrete representation learning. 30 (2017).

[60] Peng Wang and Yichun Shi. 2023. ImageDream: Image-Prompt Multi-view Diffusion for 3D Generation. *arXiv preprint arXiv:2312.02201* (2023).

[61] Tengfei Wang, Bo Zhang, Ting Zhang, Shuyang Gu, Jianmin Bao, Tadas Baltrušaitis, Jingjing Shen, Dong Chen, Fang Wen, Qifeng Chen, et al. 2023. Rodin: A generative model for sculpting 3d digital avatars using diffusion. 4563–4573.

[62] Zhou Wang, Alan C Bovik, Hamid R Sheikh, and Eero P Simoncelli. 2004. Image quality assessment: from error visibility to structural similarity. *IEEE transactions on image processing* 13, 4 (2004), 600–612.

[63] Zhengyi Wang, Jonathan Lorraine, Yikai Wang, Hang Su, Jun Zhu, Sanja Fidler, and Xiaohui Zeng. 2024. LLaMA-Mesh: Unifying 3D Mesh Generation with Language Models. *arXiv preprint arXiv:2411.09595* (2024).

[64] Zhengyi Wang, Cheng Lu, Yikai Wang, Fan Bao, Chongxuan Li, Hang Su, and Jun Zhu. 2023. Prolificdreamer: High-fidelity and diverse text-to-3d generation with variational score distillation. 36 (2023), 8406–8441.

[65] Zhenwei Wang, Tengfei Wang, Zexin He, Gerhard Petrus Hancke, Ziwei Liu, and Rynson WH Lau. 2025. Phidias: A Generative Model for Creating 3D Content from Text, Image, and 3D Conditions with Reference-Augmented Diffusion.

[66] Si-Tong Wei, Rui-Huan Wang, Chuan-Zhi Zhou, Baoquan Chen, and Wang Peng-Shuai. 2025. OctGPT: Octree-based Multiscale Autoregressive Models for 3D Shape Generation. In *SIGGRAPH*.

[67] Shuang Wu, Youtian Lin, Feihu Zhang, Yifei Zeng, Jingxi Xu, Philip Torr, Xun Cao, and Yao Yao. 2024. Direct3D: Scalable Image-to-3D Generation via 3D Latent Diffusion Transformer. *arXiv preprint arXiv:2405.14832* (2024).

[68] Jiale Xu, Weihao Cheng, Yiming Gao, Xintao Wang, Shenghua Gao, and Ying Shan. 2024. Instantmesh: Efficient 3d mesh generation from a single image with sparse-view large reconstruction models. *arXiv preprint arXiv:2404.07191* (2024).

[69] Lijun Yu, Jose Lezama, Nitesh Bharadwaj Gundavarapu, Luca Versari, Kihyuk Sohn, David Minnen, Yong Cheng, Agrim Gupta, Xiuye Gu, Alexander G Hauptmann, et al. 2024. Language Model Beats Diffusion-Tokenizer is key to visual generation. (2024).

[70] Biao Zhang, Jiapeng Tang, Matthias Niessner, and Peter Wonka. 2023. 3dshape2vecset: A 3d shape representation for neural fields and generative diffusion models. *ACM Transactions on Graphics* 42, 4 (2023), 1–16.

[71] Longwen Zhang, Ziyu Wang, Qixuan Zhang, Qiwei Qiu, Anqi Pang, Haoran Jiang, Wei Yang, Lan Xu, and Jingyi Yu. 2024. CLAY: A Controllable Large-scale Generative Model for Creating High-quality 3D Assets. *ACM Transactions on Graphics (TOG)* 43, 4 (2024), 1–20.

[72] Richard Zhang, Phillip Isola, Alexei A Efros, Eli Shechtman, and Oliver Wang. 2018. The unreasonable effectiveness of deep features as a perceptual metric. In *Proceedings of the IEEE conference on computer vision and pattern recognition*. 586–595.

[73] Xuying Zhang, Yutong Liu, Yangguang Li, Renrui Zhang, Yufei Liu, Kai Wang, Wanli Ouyang, Zhiwei Xiong, Peng Gao, Qibin Hou, and Ming-Ming Cheng. 2025. Tar3d: Creating high-quality 3d assets via next-part prediction. (2025), 5134–5145.

[74] Xuying Zhang, Yupeng Zhou, Kai Wang, Yikai Wang, Zhen Li, Shaohui Jiao, Daquan Zhou, Qibin Hou, and Ming-Ming Cheng. 2025. Ar-1-to-3: Single image to consistent 3d object generation via next-view prediction. *arXiv preprint arXiv:2503.12929* (2025).